Author Manuscript

Author Manuscript

Author Manuscript

Author Manuscript

HHS Public Access

Author manuscript

Biochim Biophys Acta Mol Basis Dis. Author manuscript; available in PMC 2023 January 01.

Published in final edited form as:

Biochim Biophys Acta Mol Basis Dis. 2022 January 01; 1868(1): 166278. doi:10.1016/j.bbadis.2021.166278.

Endothelial Cell-Derived Pro-fibrotic Factors Increase TGF-β1 Expression by Smooth Muscle Cells in Response to Cycles of Hypoxia-Hyperoxia

Ahmed Ismaeel, PhD[1], **Dimitrios Miserlis, MD**[2], **Evlampia Papoutsi, MS**[1], **Gleb Haynatzki, PhD**[3], **William T. Bohannon, MD**[4], **Robert S. Smith, MD**[4], **Jack L. Eidson, MD**[4], **George P. Casale, PhD**[5], **Iraklis I. Pipinos, MD**[5], **Panagiotis Koutakis, PhD**[1,*]

[1]Department of Biology, Baylor University, Waco, TX, B.207 Baylor Science Building, One Bear Place #97388, Waco, TX 76798-7388

[2]Department of Surgery, University of Texas Health Science Center San Antonio, San Antonio, TX, 8300 Floyd Curl Dr., San Antonio, TX 78229

[3]Department of Biostatistics, University of Nebraska Medical Center, Omaha, NE, 984375 Nebraska Medical Center, Omaha, NE 68198-4375

[4]Department of Surgery, Baylor Scott & White Medical Center, Temple, TX, 2401 S 31st St, Temple, TX 76508

[5]Department of Surgery, University of Nebraska Medical Center, Omaha, NE, 982500 Nebraska Medical Center, Omaha, NE 68198-2500, USA

Abstract

Background: The vascular pathology of peripheral artery disease (PAD) encompasses abnormal microvascular architecture and fibrosis in response to ischemia-reperfusion (I/R) cycles. We aimed to investigate the mechanisms by which pathological changes in the microvasculature direct fibrosis in the context of I/R.

*Corresponding Author: Panagiotis_koutakis@baylor.edu, 254.710.2911.

Credit author statement

Contributors: Conceptualization: Ahmed Ismaeel, George P. Casale, Iraklis I. Pipinos, Panagiotis Koutakis; Methodology: Ahmed Ismaeel, Dimitrios Miserlis, Panagiotis Koutakis; Investigation: Ahmed Ismaeel, Dimitrios Miserlis, Evlampia Papoutsi, William T. Bohannon, Robert S. Smith, Jack L. Eidson; Formal analysis: Gleb Haynatzki; Data curation: Evlampia Papoutsi, Gleb Haynatzki; Resources: Dimitrios Miserlis, William T. Bohannon, Robert S. Smith, Jack L. Eidson; Supervision: Panagiotis Koutakis, William T. Bohannon; Visualization: Ahmed Ismaeel, Panagiotis Koutakis; Writing-original draft: Ahmed Ismaeel, George P. Casale, Iraklis I. Pipinos, Panagiotis Koutakis; Writing-review & editing: Dimitrios Miserlis, Evlampia Papoutsi, Gleb Haynatzki, William T. Bohannon, Robert S. Smith, Jack L. Eidson; funding acquisition: Panagiotis Koutakis.

Data Sharing Statement: The data underlying this article are available in the article and in its online supplementary material. Any additional data will be provided at a reasonable request to the corresponding author.

Declaration of interests

The authors declare that they have no known competing financial interests or personal relationships that could have appeared to influence the work reported in this paper.

Publisher's Disclaimer: This is a PDF file of an unedited manuscript that has been accepted for publication. As a service to our customers we are providing this early version of the manuscript. The manuscript will undergo copyediting, typesetting, and review of the resulting proof before it is published in its final form. Please note that during the production process errors may be discovered which could affect the content, and all legal disclaimers that apply to the journal pertain.

Author Manuscript Author Manuscript Author Manuscript Author Manuscript

Methods: Primary human aortic endothelial cells (ECs) were cultured under cycles of normoxia-hypoxia (NH) or normoxia-hypoxia-hyperoxia (NHH) to mimic I/R. Primary human aortic smooth muscle cells (SMCs) were cultured and treated with media from the ECs.

Findings: The mRNA and protein expression of the pro-fibrotic factors platelet derived growth factor (PDGF)-BB and connective tissue growth factor (CTGF) were significantly upregulated in ECs undergoing NH or NHH cycles. Treatment of SMCs with media from ECs undergoing NH or NHH cycles led to significant increases in TGF-β1, TGF-β pathway signaling intermediates, and collagen expression. Addition of neutralizing antibodies against PDGF-BB and CTGF to the media blunted the increases in TGF-β1 and collagen expression. Treatment of SMCs with PAD patient-derived serum also led to increased TGF-β1 levels.

Interpretation: In an *in-vitro* model of I/R, which recapitulates the pathophysiology of PAD, increased secretion of PDGF-BB and CTGF by ECs was shown to be predominantly driving TGF-β1-mediated expression by SMCs. These cell culture experiments help elucidate the mechanism and interaction between ECs and SMCs in microvascular fibrosis associated with I/R. Thus, targeting these pro-fibrotic factors may be an effective strategy to combat fibrosis in response to cycles of I/R.

Funding: National Institute on Aging at the National Institutes of Health grant number R01AG064420.

Graphical abstract

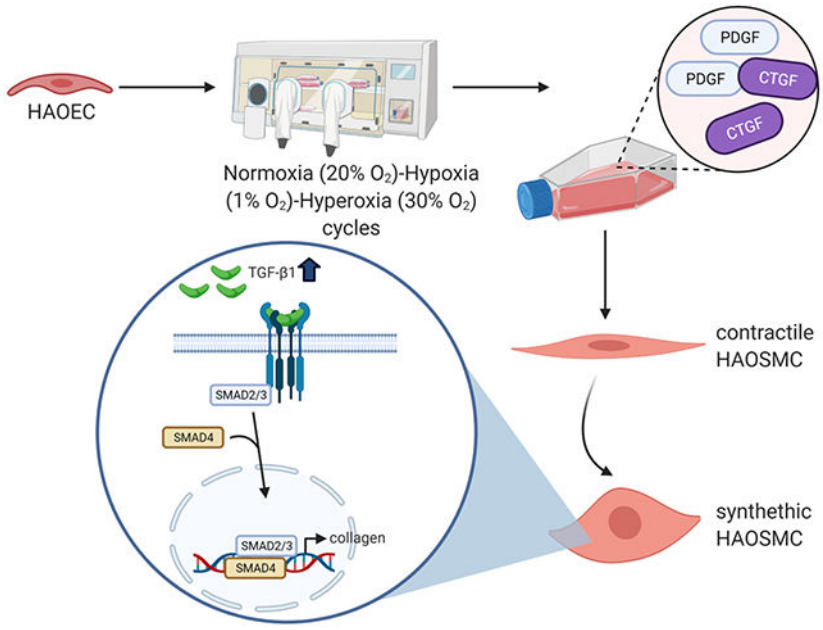

Keywords

peripheral artery disease; oxidative stress; fibrosis; microvascular pathology

Author Manuscript Author Manuscript Author Manuscript Author Manuscript

Introduction

Peripheral artery disease (PAD) refers to a group of diseases that affect arteries other than those supplying the heart and brain, the most common cause of which is atherosclerosis (1). PAD is associated with increased cardiovascular burden as well as exercise limitations, and even asymptomatic patients experience severe reductions in exercise performance (2). The pathophysiology of the functional impairment associated with PAD is believed to be linked to oxidative stress (3). During activity, PAD patients experience limb ischemia, and the temporary lack of oxygen causes an accumulation of oxidative phosphorylation precursors and reducing equivalents, and allows electrons to be more available for reduction (4). At rest, oxygen is reintroduced, accompanied by an increase in reactive oxygen species (ROS) production and oxidative stress, a process known as ischemia-reperfusion (I/R) injury (5). Oxidative stress in PAD patients has been linked to a skeletal muscle myopathy, characterized by myofiber atrophy and build-up of connective tissue between myofibers and myofasicles, or myofibrosis (6).

There are several mechanisms by which chronic I/R may induce fibrosis, which all converge on the increased expression and activation of transforming growth factor-beta 1 (TGF-β1), the most potent inducer of pathological fibrosis (7). Transcriptomic analysis of muscle biopsies identified TGF-β signaling-associated pathways as gene expression features of PAD (8). Studies of gastrocnemius biopsies from PAD patients have also shown increased TGF-β1 expression characteristically limited to microvasculature, correlating with collagen density (9, 10). Co-localization studies of TGF-β1 and candidate cell markers revealed that vascular smooth muscle cells (SMCs) exclusively expressed TGF-β1 (9). SMCs are known to transform from a contractile to synthetic phenotype, characterized by decreased contractile proteins and increased migratory and proliferative potential, and synthetic SMCs are known to produce TGF-β1 (11). One of the major drivers of this de-differentiation process is the exposure of SMCs to growth factors, including platelet derived growth factor (PDGF)-BB and connective tissue growth factor (CTGF) (12). Notably, oxidative stress has been shown to enhance cellular secretion of PDGF-BB (13) and CTGF (14). Vascular endothelial cells (ECs) have been found to secrete PDGF-BB and CTGF, which can modulate responses in SMCs (15, 16).

In the present work, we hypothesized that cycles of I/R would induce fibrosis by oxidative damage to ECs that release pro-fibrotic paracrine factors PDGF-BB and CTGF, which act to increase dedifferentiation of SMCs to a synthetic phenotype that releases TGF-β1. We tested this hypothesis using a novel *in-vitro* cell culture model of I/R by culturing primary human vascular cells under cycles of normoxia-hypoxia (NH) or normoxia-hypoxia-hyperoxia (NHH). The use of NHH is based on near-infrared spectroscopy studies, which have shown that gastrocnemius oxygen saturation (StO2) of PAD patients is characterized by a rapid drop during exercise, followed by a sharp rise in StO2 during recovery (17) (Supplementary information (SI) Figure 1). Relative to standard cell culture oxygen levels of 20% (normoxia), a ~95% reduction in StO2 (hypoxia) was designated as 1% oxygen. Furthermore, an increase in StO2 of approximately 150% of baseline was designated as 30% oxygen during the hyperoxia phase. We also treated cells with serum from PAD patients as a validation of this model.

Author Manuscript Author Manuscript Author Manuscript Author Manuscript

Materials and Methods

EXPERIMENTAL MODEL AND SUBJECT DETAILS

Endothelial Cell Culture—Commercially purchased primary human aortic ECs (iX Cells Biotech, San Diego, CA, 10HU-020, donor sex: mixed donors) were cultured at 37°C. Culture medium consisted of EBM-2 Endothelial Cell Growth Basal Medium-2 (Lonza Group AG, Switzerland) supplemented with EGM-2 Endothelial Cell Growth Medium-2 BulletKit (Lonza Group AG), FBS to a final concentration of 20% (v/v), and 1x penicillin streptomycin (Pen-Strep) solution. Cells were plated on T-25 flasks coated with 0.1% gelatin/phosphate-buffered saline (PBS) solution (ATCC, Manassas, VA). Culture medium was collected daily and replaced with fresh medium. Cells were subcultured when cultures reached approximately 80% confluence. Cells were exposed to cycles of NH or NHH, with the OxyCycler C42, a computer-controlled system that simultaneously regulates both O_2 and CO_2 tension (Biospherix, Parish, NY) according to the following protocol: NH: 90 minutes at normoxia (N) (20% O_2, 75% N_2, 5% CO2) and 90 minutes at hypoxia (1% O_2, 94% N_2, 5% CO_2), NHH: 90 minutes at N, 60 minutes at hypoxia, and 30 minutes at hyperoxia (30% O_2, 65% N_2, 5% CO_2). Control cells were incubated under constant N. Cells were collected after 1, 3, and 5 days of the oxygen cycling conditions. Additionally, to test whether the effects of NHH persist after return to longer periods of normoxia, ECs were exposed to NHH cycles for 5 days, followed by 5 days of constant normoxia. Finally, to test whether effects of NHH could be observed with shorter exposure times, cells were exposed to normoxia for 30 minutes, hypoxia for 15 minutes, and hyperoxia for 15 minutes, for 1-, 2-, 3-, 6-, and 12-hour cycles.

Smooth Muscle Cell Culture—Primary Human Aortic SMCs (Gelantis, San Diego, CA, PH35405A, Donor Age: 33, Donor Sex: Male) were incubated under continuous N at 37°C. Culture medium consisted of Smooth Muscle Cell Growth Medium 2 containing 0.05 mL/mL fetal calf serum, 0.5 ng/mL recombinant human epidermal growth factor, 2 ng/mL recombinant human basic fibroblast growth factor, and 5 μg/mL recombinant human insulin (Promo Cell, Heidelberg, Germany).

Media (20%) from ECs cultured under N, NH, or NHH were added daily to SMC cultures. A subset of SMCs treated with media from ECs undergoing NHH cycles were also supplemented with 0.03 μg/ml anti-PDGF-BB neutralizing antibody (Sigma-Aldrich, St. Louis, MO) and 10 μg/ml anti-CTGF neutralizing antibody (PeproTech, Cranbury, NJ), added into the culture medium, according to manufacturer’s instructions.

A subset of ECs and SMCs were also cultured in standard culture medium supplemented with 5% serum from: PAD patients with intermitted claudication (IC) (n=3), PAD patients with critical limb ischemia (CLI) (n=3), or non-PAD control patients (CON) (n=3). Vascular surgeons at Baylor Scott and White Hospital recruited the patients under approved IRB protocols. This study complies with the Declaration of Helsinki, and informed consent was obtained from all participants. To obtain the serum, thirty mL of blood was obtained from each patient and control after an overnight fast. Blood was immediately centrifuged (2000 g, 10 min, 4°C), and serum was aliquoted into separate polypropylene tubes and immediately stored at −80°C until time of analysis. IC or CLI diagnosis was made after measurement of

Author Manuscript Author Manuscript Author Manuscript Author Manuscript

the ankle-brachial index (ABI) and arteriography, and all controls had normal ABIs. Patient characteristics are provided in SI Table 1.

METHOD DETAILS

Measurement of Oxygen Consumption and ROS Production—Mitochondrial respiration and hydrogen peroxide (H_2O_2) production were simultaneously measured by high-resolution respirometry using Amplex UltraRed (AmR) (Thermo Fisher, Waltham, MA) with an Oroboros Oxygraph-2k (O2k) FluoRespirometer and an O2k-Fluo LED2-Module Fluorescence-Sensor Green (Oroboros Instruments, Innsbruck, Austria) (18).

High-resolution oxygen consumption was measured at 37°C in a respiration buffer supplemented with creatine monohydrate (20 mM) using the Oroboros O2k Oxygraph (Oroboros Instruments). A substrate inhibitor titration protocol was performed, in which 2 mM malate and 10 mM glutamate were added to the chambers to measure complex I, state 2 respiration. This was followed by 4 mM ADP addition, along with 4.05 μM digitonin to permeabilize the plasma membranes, to initiate state 3 respiration. Next, 10 mM succinate was added to the chambers to stimulate electron flow through complex II as well. Rotenone (10 μM) was used to inhibit complex I, and 10 μM cytochrome c was added to test the mitochondrial membrane integrity. Finally, complex IV respiration was determined using 0.4 mM *N,N,N',N'*-tetramethyl-*p*-phenylenediamine (TMPD) and 2 mM ascorbate to-prevent TMPD auto-oxidation, as well as 5 μM antimycin A to inhibit electron flow through complex III. The respiration rate was expressed as pmol oxygen consumed per second, normalized to protein content or the number of cells in the O2k-Chamber (pmols/s/mg protein or pmols/sec/#cells).

We measured cellular hydrogen peroxide production by cells using Amplex UltraRed (AmR) (Thermo Fisher Scientific) with the Oxygraph-2k FluoRespirometer and the O2k-Fluo LED2-Module Fluorescence-Sensor Green O2k (Oroboros Instruments). The reaction of hydrogen peroxide and AmR, catalyzed by horseradish peroxidase (HRP) produces a red fluorescent compound resorufin, with an excitation/emission (ex/em) of 563 nm/587 nm. Live cells were suspended in 2 mL of respiration media consisting of 105 mM MES potassium salt, 30 mM potassium chloride (KCl), 10 mM potassium dihydrogen phosphate (KH_2PO_4), 5 mM magnesium chloride, hexahydrate ($MgCl_2.6H_2O$), and 0.5 mg/mL BSA and added to the O2k-Chamber. A 10 mM stock solution of AmR was prepared by dissolving in dimethyl sulfoxide (DMSO), and 2 μL of 10 mM AmR was titrated into the O2k-Chamber, for a final concentration of 10 μM. Additionally, a stock solution with 500 U HRP/mL (Sigma-Aldrich) in respiration media was prepared, and 4 μL was titrated into the 2 mL O2k-Chamber for a final concentration of 1 U/mL. Finally, 5 U/mL of superoxide dismutase (SOD) (Sigma-Aldrich) was added to the O2k-Chamber to generate hydrogen peroxide from superoxide. Hydrogen peroxide concentrations were determined as the change of emitted fluorescence intensity as hydrogen peroxide is consumed by AmR and normalized to the oxygen consumption rate. A standard curve of the slope of the AmR fluorescence intensity was created using calibration standards of a commercial solution of 3 wt.% hydrogen peroxide (Sigma-Aldrich) by titrating stepwise increases of 0.1 μM

Author Manuscript Author Manuscript Author Manuscript Author Manuscript

hydrogen peroxide into the O2k-Chamber. ROS production was expressed as hydrogen peroxide flux per O2k-Chamber volume (μM/s*ml or pmols/sec*ml).

Gene Expression Analysis—A RNeasy Mini Kit (Qiagen) was used to purify total RNA. RNA concentrations were determined using a NanoDrop One Microvolume UV-Vis Spectrophotometer (Thermo Fisher Scientific). The RNeasy Mini Kit (Qiagen) was used to purify total RNA from approximately 1 x 10^6 cells. A RT^2 First Strand Kit (Qiagen) was used for cDNA synthesis from an RNA concentration of 0.5 μg total RNA for reverse transcription. Real-time PCR using a RT^2 Profiler PCR Array (Qiagen, Hilden, Germany) in combination with RT^2 SYBR Green Mastermix (Qiagen) run on a QuantStudio 3 PCR System (Thermo Fisher) was used for analysis of mRNA expression. Specifically, the Human Fibrosis RT^2 Profiler PCR Array (PAHS-120ZA) was used to determine the relative expression of 84 genes involved in the fibrotic process. The GeneGlobe Data Analysis Center (Qiagen) was used to calculate threshold cycle (C_T) values between genes of interest and reference ("housekeeping genes") genes to normalize data. The 2^ (-delta delta C_T) method was used to calculate fold change (19).

Protein Analysis—For protein extraction, cells were resuspended in ice-cold lysis buffer, consisting of 50 mM Tris-HCl at pH 7.4, 150 mM NaCl, 1% NP-40, 0.25% Na-deoxycholate, 0.1% SDS, and 1x protease inhibitor cocktail (diluted 1:100 in lysis buffer) and then sonicated with a Biorupter sonicator (Diagenode SA, Belgium) for 5 cycles of 30 seconds on and 30 seconds off at 4°C. To measure protein concentration in samples, a Pierce BCA Protein Assay Kit (Thermo Fisher) was used. For western blotting, protein samples were mixed with 4x NuPAGE LDS Sample Buffer and 10x NuPAGE Reducing Agent (Thermo Fisher), and then using NuPAGE 4-12% Bis-Tris gels, equal amounts of protein (10 μg) were separated using electrophoresis in a Mini Gel Tank (Thermo Fisher). Proteins were transferred to Immobilon-P polyvinylidene difluoride (PVDF) transfer membranes (MilliporeSigma, Burlington, MA) and incubated in primary antibodies (Abcam, Cambridge, UK), followed by incubation with appropriate HRP-conjugated secondary antibody. Membranes were visualized using Clarity ECL Substrate (Bio-Rad, Hercules, CA), and bands were detected using the ChemiDoc MP Imaging System (Bio-Rad). Band intensities were quantified using Image Lab (Bio-Rad).

For quantitative measurement of PDGF-BB and Pro-Collagen I α1 (COL1A1), commercial sandwich ELISAs were used (PeproTech and R&D Systems, Minneapolis, MN, respectively) according to manufacturer's recommendations. The PDGF-BB concentrations in samples were determined by comparing their absorbance to a known recombinant PDGF-BB standard curve. The range of the kit is 16-1000 pg/ml. The intra-assay CV was determined as 3.7%. To measure COL1A1, the DuoSet ELISA Human Pro-Collagen 1 alpha 1 (R&D Systems) was used. The range of the kit is 31.2-2000 pg/ml. All samples, controls, and standards were assayed in duplicate. The intra-assay CV was determined as 2.1%. The optical density of wells was determined using a ELx808 absorbance microplate reader set to 450 nm (BioTek, Winooski, VT).

Imaging and Immunofluorescence—To measure mitochondrial ROS, we used MitoSOX Red mitochondrial superoxide indicator (Thermo Fisher) by fluorescence

Author Manuscript Author Manuscript Author Manuscript Author Manuscript

microscopy. MitoSOX is targeted to the mitochondria, and oxidation of this reagent by superoxide can be detected at an ex/em of 510/580 nm (red). For all immunofluorescence experiments, quantification was based on two- or three-channel imaging of each microscopic field. Three microscopic fields (approximately 10-20 cells per field) were analyzed from each of three different wells for a total of 6 fields for each condition. The mean fluorescence signal was expressed as mean pixel intensity in grayscale units on a 12-bit gray scale, corrected for background.

To measure lipid peroxidation, we used a Cell-based Lipid Peroxidation Assay Kit (Abcam). This kit uses a sensor that changes fluorescence from red to green upon peroxidation. For the Cell-based Lipid Peroxidation Assay Kit first, a 10x working solution of the lipid peroxidation sensor was prepared by diluting in Hank's Buffer with Hepes (HHBS). Lipid peroxidation sensor was then added to the cells at a final concentration of 1x. Cells were incubated for 30 minutes at 37°C. The media was then removed, and cells were washed with HHBS 3 times. Following washes, the fluorescence of the cells was monitored within 2 hours of staining. Data were represented as the ratios of red/green. Mitochondrial ROS was expressed as the ratio of the mean MitoSOX fluorescence signal over the mean MitoTracker signal. Fluorescence images were captured with an EVOS FL Auto Imaging System (Thermo Fisher).

Cell Adhesion Assay—The Vybrant Cell Adhesion Assay Kit (Thermo Fisher) was used to measure EC adhesion to microplate wells coated with Type I collagen solution (RatCol Rat Tail Collagen, Advanced BioMatrix, at a working concentration of 35 μg/ml. Microplate wells were incubated at room temperature, covered, for 1-2 hours with the diluted Rat Tail collagen added to the well surface. Remaining material was aspirated, and coated surfaces were rinsed with PBS. Cells were resuspended in serum-free medium at 5 x 10^6 cells/ml, and then calcein AM stock solution was added to cell suspensions at a concentration of 5 μM. Cells were incubated for 30 minutes at 37°C, washed twice with serum-free medium, and then 100 μL of the calcein-labeled cell suspension was added to the coated microplate wells. Cells were incubated for 120 minutes at 37°C, followed by removal of nonadherent calcein-labeled cells by 5 washes. Fluorescence was then measured with a Varioskan LUX Multimode Microplate Reader (Thermo Fisher) at an Ex/Em of 494 nm/517 nm. The percentage of adhesion was calculated by dividing background-subtracted fluorescence of adherent cells by the total corrected fluorescence of cells added to each microplate well, multiplied by 100%.

Gastrocnemius Evaluation—Human Fibrosis RT^2 Profiler PCR Arrays were also used for the quantitative analysis of gene expression signatures of gastrocnemius biopsies from the CLI patients (n=3), and CON patients (n=3) described above. Biopsies were obtained from the anteromedial segment of the gastrocnemius muscle in the more symptomatic limb using a Magnum Biopsy Instrument and needle (Bard, Covington, GA).

QUANTIFICATION AND STATISTICAL ANALYSIS

Each experiment was performed in triplicate, and results from 3 independent experiments were averaged. All data are expressed as means ± standard deviations (SD). All statistical

Author Manuscript Author Manuscript Author Manuscript Author Manuscript

analyses were performed with SPSS 26 (IBM, Armonk, NY) or GeneGlobe Data Analysis Center with a 95% confidence level (α=0.05).

For all biological parameters except gene expression, group differences were determined by a one-way analysis of variance (ANOVA) and evaluated post-hoc by Bonferroni adjusted t-tests. For PCR array data, p-values were calculated based on a Student's t-test of the replicate 2^(-Delta C_T) values for each gene in the control and treatment groups. The p-value calculation used was based on parametric, unpaired, two-sample equal variance, two-tailed distribution. Protein levels were expressed as fold changes of the protein adjusted to the loading control, GAPDH, relative to the control condition. The null hypothesis that group means are equal in terms of each parameter was tested against the alternative hypothesis that at least one group/condition mean is different. The assumptions of normality and homogeneity of variances were verified prior to analysis. Equal variances were verified using descriptive and Levene's test. In the case of a normality violation, the Kruskal-Wallis test was used in place of the one-way ANOVA. In the case of a violation of equal variances, Welch's adjustment was used.

Reagent Identification

REAGENT OR RESOURCE	SOURCE	IDENTIFIER
Cells		
Human Aortic Endothelial Cells	iXCells Biotech	10HU-020
Human Aortic Smooth Muscle Cells	Genlantis	PH35405A
PCR Array		
Human Fibrosis RT2 Profiler	Qiagen	PAHS-120ZA (330231)
Antibodies (Western blot)		
Anti-NOX2	Abcam	Ab129068
Anti-HIF-1α	Abcam	Ab1
Anti-CTGF	Abcam	Ab227180
Anti-TGF beta 1	Abcam	Ab179695
Anti-vimentin	Abcam	Ab137321
Anti-calponin 1	Abcam	Ab46794
Anti-alpha smooth muscle actin	Abcam	Ab7817
Anti-GAPDH	Abcam	Ab9485
Anti-PDGF-BB	Abcam	Ab9704
Antibodies (Neutralizing)		
Anti-PDGF-BB	Sigma-Aldrich	07-1437
Anti-CTGF	PeproTech	500-P252
ELISA		
Human PDGF-BB Mini ABTS ELISA Development Kit	PeproTech	900-M04
DuoSet ELISA Human Pro-Collagen 1 alpha 1	R&D Systems	DY6220-05
Assays		

Author Manuscript Author Manuscript Author Manuscript Author Manuscript

REAGENT OR RESOURCE	SOURCE	IDENTIFIER
MitoSOX Red	Thermo Fisher	M36008
Lipid Peroxidation Assay Kit (Cell-based)	Abcam	Ab243377
Vybrant Cell Adhesion Assay Kit	Thermo Fisher	V13181

Results

Cycles of NH and NHH Increase ROS Production and Reduce Mitochondrial Function in ECs

Live-cell H_2O_2 production during respiration was significantly higher in ECs after 5 days of NH during complex II, state 3 respiration (CII_3) ($p<0.001$) and complex IV, state 3 respiration (CIV_3) ($p<0.001$) compared to N (Figure 1a). Following 5 days of NHH, ROS production was significantly elevated during complex I, state 2 respiration (CI_2) ($p=0.04$), CII_3 ($p<0.001$), and CIV_3 ($p<0.001$) as well.

Likewise, after 3 days of NH, ROS production was significantly greater during CI_2 ($p<0.001$), combined complex I and complex II respiration (CI+II) ($p<0.001$), and CII_3 ($p=0.034$) compared to N (SI Figure 2a). Furthermore, after 1 day of NHH, ROS production was increased during CII_3 ($p<0.001$). Following 3 days of NHH, ROS production was greater during CII_3 ($p<0.001$) and CIV_3 ($p<0.001$) as well.

Consistent with mitochondrial dysfunction, oxygen flux ($JO2$), a direct measure of oxygen consumption rate (OCR), was significantly reduced during CI_2 in ECs undergoing NH and NHH cycles for 5 days compared to constant N ($p=0.012$ and $p=0.006$, respectively) (Figure 1b). After the addition of digitonin to permeabilize the plasma membrane and exogenous ADP (CI_3 exogenous), as well as during CI+II, OCR was significantly lower in ECs undergoing NH or NHH for 5 days ($p<0.001$ for both).

OCR was also reduced during CI_2 following 1 and 3 days of NH and NHH ($p=0.004$, $p=0.001$, $p=0.001$, $p=0.001$, respectively) (SI Figure 2b). During CI_3 endogenous respiration, OCR was lower in ECs undergoing NH for 3 days ($p=0.016$) as well as NHH for 1 and 3 days ($p=0.022$ and $p=0.016$, respectively). OCR was also reduced during CI_3 exogenous respiration following NH and NHH cycles for 1 and 3 days ($p<0.001$ for all). Finally, during CIV_3, OCR was significantly reduced following 1 day of NHH compared to N ($p<0.001$).

To test the effect of PAD patient serum on ECs, cells were treated with 5% serum from one of 3 IC patients, 3 CLI patients, or 3 CON patients. There were no significant differences in H_2O_2 production during the respiration of any complexes, with the exception of CIV_3 (SI Figure 3a). During CIV_3, ECs treated with IC or CLI serum both had increased ROS production compared to CON serum-treated ECs ($p=0.001$ and $p<0.001$, respectively). ECs treated with serum from IC or CLI patients displayed significantly reduced OCRs during exogenous CI_3 ($p=0.011$), CII_3 ($p=0.022$), and CIV_3 ($p=0.043$) respiration (SI Figure 3b).

Author Manuscript Author Manuscript Author Manuscript Author Manuscript

Since NADPH oxidase 2 (NOX2) has been implicated a potential source of ROS in I/R (20) and PAD (21), NOX2 protein expression was measured in ECs. There was a significant upregulation in NOX2 protein expression in ECs undergoing NH or NHH for 1, 3, and 5 days compared to N (SI Figure 4a,b). Furthermore, hypoxia inducible factor- 1 alpha (HIF-1α) protein was detected in ECs undergoing NH and NHH, but not in normoxic ECs (SI Figure 4c).

Cycles of NH and NHH Increase the Expression of Pro-fibrotic Factors in ECs

Of the genes assessed by the Human Fibrosis RT^2 Profiler PCR Array, the following inflammatory genes were significantly upregulated in ECs after 5 days of NH relative to N: *CCL2* (9.21 ± 1.85-fold, p<0.001), *CXCR4* (3.35 ± 1.57-fold, p=0.047), *IL1A* (10.43 ± 2.60-fold, p<0.001), and *NFKB1* (4.35 ± 1.10-fold, p=0.006) (Figure 2a). After 5 days of NHH cycles, the following genes were significantly upregulated relative to N: *CCL2* (8.54 ± 2.80-fold, p<0.001), *CXCR4* (4.91 ± 1.67-fold, p=0.048), *IL13RA2* (2.25 ± 0.40-fold, p=0.04), *IL1A* (17.25 ± 2.72-fold, p<0.001), *IL1B* (3.42 ± 1.08-fold, p=0.003), and *NFKB1* (3.58 ± 1.17-fold, p=0.02). Furthermore, consistent with enhanced inflammation, ECs undergoing NHH for 5 days demonstrated significantly enhanced cell adhesion (p=0.04) (SI Figure 4d).

In addition, in ECs undergoing NH and NHH for 5 days, the cellular mRNA expression of *CTGF* (8.41 ± 1.75-fold, p<0.001; and 4.92 ± 1.13-fold, p<0.001, respectively) and *PDGFB* (2.99 ± 1.07-fold, p=0.03; and 13.11 ± 3.35-fold, p=0.001, respectively) were significantly elevated relative to N (Figure 2a). No other genes were significantly different between conditions. The remainder of the PCR array data are provided in SI Table 2. Furthermore, secreted PDGF-BB concentrations were significantly higher in the media from ECs undergoing cycles of NH for 3 days (192.45 ± 1.25 pg/ml, p<0.001) and 5 days (155.95 ± 0.75 pg/ml, p=0.001), as well as NHH for 1 day (128.45 ± 0.25, p<0.001) and 5 days (403.45 ± 61.25 pg/ml, p<0.001), relative to N (18.7 ± 2.8 pg/ml) (Figure 2b). Likewise, secreted CTGF protein expression was significantly upregulated, relative to N, in ECs following 1 day of NH (2.53 ± 0.06-fold, p=0.004), 3 days of NH (4.80 ± 0.16-fold, p<0.001), 3 days of NHH (7.35 ± 0.84-fold, p<0.001), and 5 days of NHH (3.68 ± 0.28-fold, p<0.001) (Figure 2c,d). Interestingly, shorter exposure times of NHH cycles were also sufficient to increase PDGF-BB and CTGF secretion. ECs undergoing NHH for 1-, 3-, 6-, and 12-hour cycles showed significant elevations in secreted PDGF-BB and CTGF protein expression compared to N (SI Figure 5). Furthermore, secreted PDGF-BB and CTGF levels remained elevated in ECs undergoing NHH, even after a return to normoxia for a period of 5 days.

Similarly, ECs treated with serum from IC or CLI patients demonstrated significantly greater CTGF mRNA expression relative to CON serum-treated ECs (p=0.04 and p=0.02, respectively) (SI Figure 6a). Additionally, CLI serum-treated ECs showed significantly enhanced mRNA expression of *IL13* (p=0.01), *IL1A* (p=0.02), and *PDGFB* (p=0.01), as well as secretion of PDGF-BB (p=0.002) (SI Figure 6b) and CTGF (p<0.001) (SI Figure 6c,d). However, secretion of PDGF-BB and CTGF was not different between IC serum-

Author Manuscript Author Manuscript Author Manuscript Author Manuscript

treated ECs and CON serum-treated ECS. The remainder of the PCR array data for the serum-treated ECs are provided in SI Table 3.

Treatment of SMCs with PAD Serum Increases ROS Production and Oxidative Damage

There were no significant differences in JO2 between SMCs treated with 5% serum from IC or CON patients. However, the OCR was significantly lower in SMCs treated with serum from CLI patients during CI_2 ($p<0.001$), CI_3 (exogenous) ($p=0.004$), and CIV_3 ($p=0.011$) respiration compared to CON (Figure 3a). H_2O_2 production was significantly higher in SMCs treated with IC or CLI serum compared to SMCs treated with CON serum during CI_3 (exogenous) ($p=0.031$ and $p=0.023$, respectively) and CIV_3 ($p=0.05$ and $p=0.01$, respectively). In CLI serum-treated SMCs, H_2O_2 production was further elevated during CI_2 and CII_3 ($p=0.018$ and $p=0.035$, respectively) (Figure 3b). SMCs treated with serum from IC and CLI patients also demonstrated significantly greater mitochondrial superoxide, detected by MitoSOX (Figure 4a,b) and lipid peroxidation, quantified by a sensitive ratiometric sensor (Figure 4c,d) compared to SMCs treated with CON serum.

Fibrotic Phenotype in SMCs Treated with Media from ECs undergoing NH and NHH Cycles

SMCs were treated with 20% media from ECs that were cultured under N or NHH cycles for 5 days. The relative expression of the following genes was significantly elevated in SMCs treated with media from ECs undergoing NHH compared to N: *COL1A2* (4.11 ± 0.83-fold, p=0.006), *ITGA3* (3.04 ± 0.57-fold, p=0.007), *ITGB5* (3.60 ± 0.77-fold, p=0.01), *MMP3* (3.96 ± 1.54-fold, p=0.03), *SMAD2* (8.36 ± 4.10-fold, p=0.04), *SMAD3* (5.27 ± 2.59-fold, p=0.04), *SMAD6* (5.11 ± 1.80-fold, p=0.02), *TGFB1* (8.36 ± 3.94-fold, p=0.04), *TGFBR1* (3.86 ± 1.15-fold, p=0.03), and *TGFBR2* (4.18 ± 1.75-fold, p=0.04) (Figure 5a). However, supplementation of the media from ECs undergoing NHH with an anti-PDGF-BB and an anti-CTGF neutralizing antibody abolished the increase in *ITGA3* (0.79 ± 0.26-fold, p=0.47 vs EC N media), *MMP3* (1.26 ± 0.21-fold, p=0.44), *SMAD2* (1.93 ± 1.13-fold, p=0.26), *SMAD3* (1.11 ± 0.48-fold, p=0.73), *TGFB1* (1.93 ± 0.51-fold, p=0.57), *TGFBR1* (0.24 ± 0.79-fold, p=0. 43), and *TGFBR2* (1.93 ± 1.81-fold, p=0.43). The complete PCR array data are provided in SI Table 4. Likewise, the protein expression of COL1A1 was significantly elevated in SMCs treated with media from ECs cultured under NHH cycles compared to N (1.92 ± 0.04-fold, p=0.003), and supplementation of the media with neutralizing antibodies against PDGF-BB and CTGF abrogated this increase (0.94 ± 0.04-fold, p=0.981) (Figure 5b). Similarly, the protein expression of TGF-β1 was significantly elevated following treatment with media from ECs undergoing NHH (2.5-fold compared to EC N media, $p<0.001$), and supplementation of the media with anti-PDGF-BB/CTGF antibodies prevented this increase (1.08-fold, p=0.702 compared to EC N) (Figure 5c,d). The protein expression of TGF-β1 was also significantly upregulated in SMCs treated with serum from IC (4.92 ± 0.29-fold, p=0.021) or CLI (6.64 ± 2.17-fold, p=0.004) patients compared to CON serum-treated SMCs (SI Figure 7).

To investigate whether treatment of SMCs with media from ECs undergoing NHH causes the cells to undergo a phenotypic switch from contractile to synthetic, we measured the protein expression of the contractile markers calponin-1 and α-smooth muscle actin (α-SMA), and the synthetic SMC marker, vimentin. Interestingly, relative to untreated, control

Author Manuscript Author Manuscript Author Manuscript Author Manuscript

SMCs cultured under standard conditions, SMCs treated with media from normoxic ECs showed a significant reduction in vimentin expression (0.48 ± 0.10-fold, p<0.001) (Figure 6a,b) and a significant increase in calponin-1 expression (6.28 ± 0.08-fold, p<0.001) (Figure 6a,c). In contrast, SMCs treated with media from ECs cultured under NHH demonstrated significant elevations in vimentin expression (3.72 ± 0.12-fold, p<0.001). Calponin-1 expression was also significantly reduced relative to SMCs treated with media from ECs undergoing N (p<0.001). Supplementation of the EC NHH media with neutralizing antibodies against PDGF-BB and CTGF blunted the increase in vimentin expression (p<0.001 vs. NHH) as well as the reduction in calponin-1 expression (p<0.001 vs. NHH).

Fibrotic Phenotype in Gastrocnemius Biopsies of CLI Patients

To determine whether our *in vitro* fibrotic expression matches the skeletal muscle gene expression of patients, we used the Human Fibrosis RT^2 Profiler PCR Array to assess the relative expression of selected fibrotic genes in gastrocnemius samples from 6 PAD patients (3 IC and 3 CLI) compared to the 3 CON. Several fibrosis-related genes were significantly elevated in PAD muscle compared to CON that resembled the mRNA expression of the ECs and SMCs, including *CXCR4* (2.42 ± 0.17-fold, p=0.037), *CTGF* (2.22 ± 0.19-fold, p=0.048), *MMP3* (3.01 ± 1.13-fold, p=0.028), *PDGFB* (2.86 ± 0.36-fold, p=0.046), *TGFB1* (2.59 ± 0.26-fold, p=0.036), and *TGFBR2* (2.57 ± 0.21-fold, p=0.025) (Figure 7). The complete PCR array data are provided in SI Table 5.

Discussion

Our first finding of the present study was that 3 and 5 days of NH or NHH cycles increased EC H_2O_2 production during the respiration of several complexes. It has been well-known that I/R is associated with increased mitochondrial ROS production (22), and recent research has provided insights into the mechanisms. Specifically, evidence suggests that fumarate builds up during ischemia due to activation of the purine nucleotide cycle by AMP, as well as reversal of the malate/aspartate shuttle due to an elevation in the NADH/NAD ratio (23). This fumarate is in turn converted into succinate by reversal of the succinate dehydrogenase enzyme, which leads to succinate accumulation (23). When oxygen is reintroduced, succinate dehydrogenase quickly re-oxidizes succinate, which leads to reverse electron transport at complex I and elevated ROS production (23). Other mechanisms that are thought to increase ROS production during I/R include conversion of xanthine dehydrogenase to xanthine oxidase during ischemia, which is followed by reaction of molecular oxygen with hypoxanthine and xanthine oxidase during reperfusion, resulting in an increase in superoxide and hydrogen peroxide (24). Thus, although re-oxygenation of ischemic tissue is critical, it can also be detrimental when oxygen is converted into ROS such as superoxide, a phenomenon that has been termed “the oxygen paradox” (25). Several studies have consistently demonstrated that PAD patients exhibit higher levels of oxidative stress markers in circulation compared to non-PAD controls at rest as well as in response to exercise (26, 27). Likewise, there is clear evidence of oxidative stress in skeletal muscle as well (28). Increased mitochondrial ROS production can also damage mitochondrial DNA (mtDNA) (29). Therefore, ROS originating from the nearby electron transport chain can result in impaired activity of the complexes as well as further ROS production by the

Author Manuscript Author Manuscript Author Manuscript Author Manuscript

complexes (30). In this study, exposing ECs to cycles of NH or NHH (for 1-5 days) reduced the OCR, mostly during complex I, state 2 respiration and complex I, state 3 respiration compared to ECs cultured under constant N. Interestingly, reduced mitochondrial respiration has been demonstrated in gastrocnemius muscle of PAD patients, and the major affected ETC complex has been shown to be complex I (31). Muscle progenitor cells isolated from PAD gastrocnemius have also been shown to have decreased mitochondrial respiration (32). Furthermore, preclinical studies of surgically induced hindlimb ischemia have also demonstrated significant reductions in mitochondrial respiratory capacity (33). Thus, the *in vitro* model of NH or NHH cycling may reflect the *in vivo* effects of I/R on mitochondrial function.

We also found that NOX2 expression is increased in ECs undergoing NH or NHH compared to N. NOXs are unique in that they are the only known enzyme family with the sole purpose of producing ROS by transferring electrons from NADPH to oxygen (34). Previous studies have shown that NOX2 expression increases in ECs in response to hypoxia (35, 36), and that NOX2 is a target of HIF-1α (37). Thus, this may explain the NOX2 upregulation in ECs cultured under NH and NHH. Research has identified that NOX2 expression is upregulated *in vivo* in mice after stroke induced by brain I/R as well as after myocardial infarction (38, 39). In mice, endothelial-specific overexpression of NOX2, resulting in a twofold increase in NOX2 expression, has been reported to induce endothelial dysfunction and hypertension (40). NOX2 has also been implicated in PAD, as levels of soluble NOX2-derived peptide (sNOX2-dp), a marker of NOX2 activation, have been shown to be elevated in serum from PAD patients (21). Endothelial function, assessed by flow-mediated dilation (FMD), is also independently associated with sNOX2-dp in PAD patients (21). Thus, NOX2-derived ROS are thought to play a role in the reduced arterial dilation characteristic of PAD (3, 41).

ECs cultured under NH or NHH showed significant elevations in *PDGFB* and *CTGF* mRNA expression compared to N. Levels of secreted PDGF-BB and CTGF were also significantly elevated in ECs undergoing NH or NHH. CTGF was first identified from conditioned medium from human umbilical vein endothelial cells (HUVECs) in 1991 (42). Since then, CTGF has been identified as a major player in tissue remodeling and fibrosis (43). Oxidative stress, induced by either hypoxia/reoxygenation, or paraquat exposure, has been shown to upregulate CTGF mRNA and protein expression in retinal pigment epithelium cells (14, 44). Likewise, *CTGF* mRNA expression was shown to be increased 48-fold in Lewis lung carcinoma cells cultured under hypoxia, and tumoral ECs were shown to be the major source of CTGF (45). ROS have also been shown to induce PDGF-BB expression in human primary pulmonary arterial ECs (46). Interestingly, pre-treatment of ECs with antioxidants or knockdown of HIF-1α abrogated ROS-induced PDGF-BB induction (46). In our study, we provide evidence that cycles of I/R may also drive increased expression of these pro-fibrotic factors by vascular aortic ECs. PDGF is recognized as one of the primary factors that mediates SMC phenotypic transitions by binding to cell surface receptors and activating signaling pathways leading to decreased contractile protein expression and increased expression of synthetic proteins such as vimentin (47). Likewise, CTGF has been shown to directly modulate SMC phenotype (48). Importantly, synthetic SMCs are known to produce TGF-β1 (49), and activation of the TGF-β signaling pathway initiates collagen accumulation that can lead to progressive fibrosis, which has earned TGF-β the title of “the

Author Manuscript Author Manuscript Author Manuscript Author Manuscript

master regulator of fibrosis" (50). Elevated TGF-β1 in the SMCs of microvessels has been observed in PAD gastrocnemius, in association with collagen density (9, 10). These TGF-β1-expressing SMCs in PAD structurally resembled synthetic SMCs (rhomboidal shape) and also expressed Ki-67 in the nuclei, a marker of cell proliferation and activation (9).

We also sought to assess the effect of treating SMCs with media from the ECs cultured under constant N or cycles of NHH for 5 days. We chose the 5 days of NHH cycling because this media was shown to have the highest levels of PDGF-BB and CTGF. Treatment of SMCs with media from ECs undergoing NHH cycles significantly increased the synthetic SMC marker, vimentin. Another interesting finding was that treatment of SMCs with media from normoxic ECs seemed to inhibit their dedifferentiation compared to control, untreated SMCs. This was evidenced by increased expression of the contractile SMC marker, calponin-1, and reduced expression of the synthetic SMC marker vimentin. This may be explained by the fact that certain EC-derived molecules such as endothelium-derived hyperpolarizing factor (EDHF) and NO are known to modulate responses in SMCs (51). For example, EC-derived NO has been shown to negatively regulate PDGF expression and cellular proliferation in SMCs (52). TGF-β1 expression was also significantly lower in SMCs treated with media from normoxic ECs compared to untreated SMCs. However, SMCs treated with media from ECs cultured under NHH demonstrated significantly greater TGF-β1 expression, concomitant with the synthetic phenotype. These SMCs also showed enhancements in the mRNA expression of several members of the TGF-β signaling pathway, including *SMAD2*, *SMAD3*, *TGFBR1*, and *TGFBR2*. The mRNA and protein expression of COL1A2 and COL1A1, respectively, was also elevated in SMCs treated with media from ECs undergoing NHH cycles. However, supplementation of the media from the ECs undergoing NHH with neutralizing antibodies against PDGF-BB and CTGF abolished the pro-fibrotic effects of the NHH media. In fact, neutralizing PDGF-BB and CTGF protected the SMCs from the elevations in the protein expression of TGF-β1, vimentin, and COL1A1, and the mRNA expression of *TGFB1*, *SMAD2*, *SMAD3*, *TGFBR1*, and *TGFBR2*. These data further implicate EC-derived PDGF-BB and CTGF in the fibrotic process, in response to cycles of I/R. In a small subset of patients (n=9), we also provide evidence that PAD gastrocnemius possesses a fibrotic gene expression profile that is distinct from non-PAD controls, featuring elevations in *PDGFB*, *CTGF*, and *TGFB1*.

It is also important to note that cycles of NH or NHH induced an upregulation of several inflammatory genes in ECs, including *CCL2*, *CXCR4*, *IL13RA2*, *IL1A*, *IL1B*, and *NFKB1*. Notably, the associated chemokines/cytokines have been shown to be increased in inflammatory profiling of PAD blood and arterial tissue (53, 54). A growing body of evidence suggests that inflammation may in fact play a role in the development and progression of PAD (55). Oxidative stress is known to be a major determinant of vascular inflammation, and ROS are known to activate several pro-inflammatory pathways (3). For example, ROS can lead to the activation of the NLRP3 inflammasome and NF-κB, and secretion of IL-1 and IL-8 (56). Furthermore, the effect of these inflammatory biomarkers on the SMCs cannot be ruled out. Inflammatory cytokines have been shown to reduce SMC relaxation via increased endothelin-1 (57). Likewise, inflammatory cytokines can lead to SMC hyperplasia, increased collagen synthesis, and enhanced elastin degradation via increased release of matrix metalloproteinases (57). Under inflammatory conditions, EC

Author Manuscript Author Manuscript Author Manuscript Author Manuscript

expression of adhesion molecules is also upregulated (58). In fact, following stimulation by cytokines, ECs synthesize various endothelial-leukocyte adhesion molecules, including E-selectin, intracellular adhesion molecule 1 (ICAM-1), and vascular cell adhesion protein 1 (VCAM-1) (58). Importantly, these molecules regulate firm adhesion of leukocytes to the endothelium and are thought to play a major role in I/R injury (59). Interestingly, in this study, we found that culturing ECs under cycles of NHH also increased extracellular matrix (ECM)-EC adhesion compared to normoxic ECs. Future studies should assess leukocyte-endothelial interactions of ECs exposed to these oxygen cycling conditions.

The novelty in this work was in identifying whether pathological changes in SMCs and ECs are predominantly driving TGF-β1-mediated fibrosis in response to I/R. This study was formulated on rigorous quantitative studies of fibrotic biomarkers in the human disease, which allowed for directed mechanistic studies, *in vitro*, that recapitulate the pathophysiology of PAD in patients. While we have previously observed associations of vascular expression of TGF-β1 and collagen deposition in tissue from PAD patients, these findings warranted these mechanistic studies to establish SMC-derived TGF-β1 as a mediator of PAD myofibrosis. Our cell culture model of cycles of NHH to mimic I/R provided a novel means to study PAD pathophysiology that is more relevant than all previous studies incubating cells under constant hypoxia.

However, several limitations of this study exist. First, a limitation of this work is that our models of NH or NHH may not represent the exact I/R oxygen conditions that the cells are exposed to. Furthermore, ischemia involves other factors in addition to hypoxia, including metabolite accumulation. In addition, the *in-vitro* nature of the experiments, and thus our culture conditions may not reflect *in-vivo* conditions, where ECs and SMCs are present in close proximity, and there may exist complex signaling interactions between the two cell types as well as other cell types essential for increasing SMC expression of TGF-β1. While the focus of these studies was ECs and vascular SMCs, the potential role of other cell types, including fibroblasts, on the fibrotic response cannot be ruled out. Furthermore, immune cells may also play an important role, as leukocyte-endothelial interactions are known features of I/R injury.

In conclusion, we provide evidence that cycles of NH or NHH increase ROS production and the secretion of PDGF-BB and CTGF in human vascular aortic ECs. EC-derived PDGF-BB and CTGF may act to transition human vascular aortic SMCs from a contractile to synthetic phenotype, which produces TGF-β1. PDGF-BB and CTGF may therefore be specific targets for anti-fibrotic therapies for I/R. Therapeutics that target these pro-fibrotic growth factors and reduce the dedifferentiation of SMCs may prevent or slow down the progression of myofibrosis.

Supplementary Material

Refer to Web version on PubMed Central for supplementary material.

Author Manuscript Author Manuscript Author Manuscript Author Manuscript

Acknowledgements:

This work was supported by the National Institute on Aging at the National Institutes of Health under [grant number R01AG064420] to [PK]. The content is solely the responsibility of the authors and does not necessarily represent the official views of the National Institutes of Health.

References

1. Kullo IJ, Rooke TW. CLINICAL PRACTICE. Peripheral Artery Disease. The New England journal of medicine. 2016;374(9):861–71. [PubMed: 26962905]
2. Gardner AW. Claudication pain and hemodynamic responses to exercise in younger and older peripheral arterial disease patients. J Gerontol. 1993;48(5):M231–6. [PubMed: 8366266]
3. Ismaeel A, Brumberg RS, Kirk JS, Papoutsi E, Farmer PJ, Bohannon WT, et al. Oxidative Stress and Arterial Dysfunction in Peripheral Artery Disease. Antioxidants (Basel). 2018;7(10).
4. Eltzschig HK, Collard CD. Vascular ischaemia and reperfusion injury. Br Med Bull. 2004;70:71–86. [PubMed: 15494470]
5. Sinning C, Westermann D, Clemmensen P. Oxidative stress in ischemia and reperfusion: current concepts, novel ideas and future perspectives. Biomark Med. 2017;11(11):11031–1040. [PubMed: 29039206]
6. Weiss DJ, Casale GP, Koutakis P, Nella AA, Swanson SA, Zhu Z, et al. Oxidative damage and myofiber degeneration in the gastrocnemius of patients with peripheral arterial disease. Journal of translational medicine. 2013;11:230. [PubMed: 24067235]
7. Ismaeel A, Kim JS, Kirk JS, Smith RS, Bohannon WT, Koutakis P. Role of Transforming Growth Factor-beta in Skeletal Muscle Fibrosis: A Review. Int J Mol Sci. 2019;20(10).
8. Cong G, Cui X, Ferrari R, Pipinos II, Casale GP, Chattopadhyay A, et al. Fibrosis Distinguishes Critical Limb Ischemia Patients from Claudicants in a Transcriptomic and Histologic Analysis. J Clin Med. 2020;9(12).
9. Ha DM, Carpenter LC, Koutakis P, Swanson SA, Zhu Z, Hanna M, et al. Transforming growth factor-beta 1 produced by vascular smooth muscle cells predicts fibrosis in the gastrocnemius of patients with peripheral artery disease. Journal of translational medicine. 2016;14:39. [PubMed: 26847457]
10. Mietus CJ, Lackner TJ, Karvelis PS, Willcockson GT, Shields CM, Lambert NG, et al. Abnormal Microvascular Architecture, Fibrosis, and Pericyte Characteristics in the Calf Muscle of Peripheral Artery Disease Patients with Claudication and Critical Limb Ischemia. J Clin Med. 2020;9(8).
11. Pan D, Yang J, Lu F, Xu D, Zhou L, Shi A, et al. Platelet-derived growth factor BB modulates PCNA protein synthesis partially through the transforming growth factor beta signalling pathway in vascular smooth muscle cells. Biochem Cell Biol. 2007;85(5):606–15. [PubMed: 17901902]
12. Kawai-Kowase K, Owens GK. Multiple repressor pathways contribute to phenotypic switching of vascular smooth muscle cells. American journal of physiology Cell physiology. 2007;292(1):C59–69. [PubMed: 16956962]
13. Ge X, Chen SY, Liu M, Liang TM, Liu C. Evodiamine inhibits PDGFBBinduced proliferation of rat vascular smooth muscle cells through the suppression of cell cycle progression and oxidative stress. Mol Med Rep. 2016;14(5):4551–8. [PubMed: 27748810]
14. Matsuda S, Gomi F, Oshima Y, Tohyama M, Tano Y. Vascular endothelial growth factor reduced and connective tissue growth factor induced by triamcinolone in ARPE19 cells under oxidative stress. Invest Ophthalmol Vis Sci. 2005;46(3):1062–8. [PubMed: 15728566]
15. Pi L, Fu C, Lu Y, Zhou J, Jorgensen M, Shenoy V, et al. Vascular Endothelial Cell-Specific Connective Tissue Growth Factor (CTGF) Is Necessary for Development of Chronic Hypoxia-Induced Pulmonary Hypertension. Front Physiol. 2018;9:138. [PubMed: 29535639]
16. Dardik A, Yamashita A, Aziz F, Asada H, Sumpio BE. Shear stress-stimulated endothelial cells induce smooth muscle cell chemotaxis via platelet-derived growth factor-BB and interleukin-1alpha. J Vasc Surg. 2005;41(2):321–31. [PubMed: 15768016]
17. Fuglestad MA, Hernandez H, Gao Y, Ybay H, Schieber MN, Brunette KE, et al. A low-cost, wireless near-infrared spectroscopy device detects the presence of lower extremity atherosclerosis

Author Manuscript Author Manuscript Author Manuscript Author Manuscript

as measured by computed tomographic angiography and characterizes walking impairment in peripheral artery disease. J Vasc Surg. 2020;71(3):946–57. [PubMed: 31445826]

18. Makrecka-Kuka M, Krumschnabel G, Gnaiger E. High-Resolution Respirometry for Simultaneous Measurement of Oxygen and Hydrogen Peroxide Fluxes in Permeabilized Cells, Tissue Homogenate and Isolated Mitochondria. Biomolecules. 2015;5(3):1319–38. [PubMed: 26131977]
19. Livak KJ, Schmittgen TD. Analysis of relative gene expression data using real-time quantitative PCR and the 2(T)(-Delta Delta C) method. Methods. 2001;25(4):402–8. [PubMed: 11846609]
20. Kleikers PWM, Wingler K, Hermans JJR, Diebold I, Altenhofer S, Radermacher KA, et al. NADPH oxidases as a source of oxidative stress and molecular target in ischemia/reperfusion injury. J Mol Med. 2012;90(12):1391–406. [PubMed: 23090009]
21. Loffredo L, Carnevale R, Cangemi R, Angelico F, Augelletti T, Di Santo S, et al. NOX2 upregulation is associated with artery dysfunction in patients with peripheral artery disease. Int J Cardiol. 2013;165(1):184–92. [PubMed: 22336250]
22. Kim K, Anderson EM, Scali ST, Ryan TE. Skeletal Muscle Mitochondrial Dysfunction and Oxidative Stress in Peripheral Arterial Disease: A Unifying Mechanism and Therapeutic Target. Antioxidants (Basel). 2020;9(12).
23. Chouchani ET, Pell VR, Gaude E, Aksentijevic D, Sundier SY, Robb EL, et al. Ischaemic accumulation of succinate controls reperfusion injury through mitochondrial ROS. Nature. 2014;515(7527):431–5. [PubMed: 25383517]
24. Granger DN. Role of xanthine oxidase and granulocytes in ischemia-reperfusion injury. Am J Physiol. 1988;255(6 Pt 2):H1269–75. [PubMed: 3059826]
25. Yellon DM, Hausenloy DJ. Myocardial reperfusion injury. N Engl J Med. 2007;357(11):1121–35. [PubMed: 17855673]
26. Signorelli SS, Katsiki N. Oxidative stress and inflammation: their role in the pathogenesis of peripheral artery disease with or without type 2 diabetes mellitus. Current vascular pharmacology. 2017.
27. Signorelli SS, Scuto S, Marino E, Xourafa A, Gaudio A. Oxidative Stress in Peripheral Arterial Disease (PAD) Mechanism and Biomarkers. Antioxidants. 2019;8(9).
28. Koutakis P, Ismaeel A, Farmer P, Purcell S, Smith RS, Eidson JL, et al. Oxidative stress and antioxidant treatment in patients with peripheral artery disease. Physiol Rep. 2018;6(7):e13650. [PubMed: 29611350]
29. Bhat HK, Hiatt WR, Hoppel CL, Brass EP. Skeletal muscle mitochondrial DNA injury in patients with unilateral peripheral arterial disease. Circulation. 1999;99(6):807–12. [PubMed: 9989967]
30. Makris KI, Nella AA, Zhu Z, Swanson SA, Casale GP, Gutti TL, et al. Mitochondriopathy of peripheral arterial disease. Vascular. 2007;15(6):336–43. [PubMed: 18053417]
31. Pipinos II, Judge AR, Zhu Z, Selsby JT, Swanson SA, Johanning JM, et al. Mitochondrial defects and oxidative damage in patients with peripheral arterial disease. Free Radic Biol Med. 2006;41(2):262–9. [PubMed: 16814106]
32. Ryan TE, Yamaguchi DJ, Schmidt CA, Zeczycki TN, Shaikh SR, Brophy P, et al. Extensive skeletal muscle cell mitochondriopathy distinguishes critical limb ischemia patients from claudicants. JCI insight. 2018;3(21).
33. Pipinos II, Swanson SA, Zhu Z, Nella AA, Weiss DJ, Gutti TL, et al. Chronically ischemic mouse skeletal muscle exhibits myopathy in association with mitochondrial dysfunction and oxidative damage. Am J Physiol Regul Integr Comp Physiol. 2008;295(1):R290–6. [PubMed: 18480238]
34. Drummond GR, Sobey CG. Endothelial NADPH oxidases: which NOX to target in vascular disease? Trends Endocrin Met. 2014;25(9):452–63.
35. Rupin A, Paysant J, Sansilvestri-Morel P, Lembrez N, Lacoste JM, Cordi A, et al. Role of NADPH oxidase-mediated superoxide production in the regulation of E-selectin expression by endothelial cells subjected to anoxia/reoxygenation. Cardiovascular Research. 2004;63(2):323–30. [PubMed: 15249190]
36. Yuan G, Khan SA, Luo W, Nanduri J, Semenza GL, Prabhakar NR. Hypoxia-inducible factor 1 mediates increased expression of NADPH oxidase-2 in response to intermittent hypoxia. Journal of cellular physiology. 2011;226(11):2925–33. [PubMed: 21302291]

Author Manuscript Author Manuscript Author Manuscript Author Manuscript

37. Kietzmann T, Gorlach A. Reactive oxygen species in the control of hypoxia-inducible factor-mediated gene expression. Semin Cell Dev Biol. 2005;16(4-5):474–86. [PubMed: 15905109]
38. Looi YH, Grieve DJ, Siva A, Walker SJ, Anilkumar N, Cave AC, et al. Involvement of Nox2 NADPH oxidase in adverse cardiac remodeling after myocardial infarction. Hypertension. 2008;51(2):319–25. [PubMed: 18180403]
39. Hong H, Zeng JS, Kreulen DL, Kaufman DI, Chen AF. Atorvastatin protects against cerebral infarction via inhibition of NADPH oxidase-derived superoxide in ischemic stroke. American journal of physiology Heart and circulatory physiology. 2006;291(5):H2210–5. [PubMed: 16766636]
40. Murdoch CE, Alom-Ruiz SP, Wang M, Zhang M, Walker S, Yu B, et al. Role of endothelial Nox2 NADPH oxidase in angiotensin II-induced hypertension and vasomotor dysfunction. Basic Res Cardiol. 2011;106(4):527–38. [PubMed: 21528437]
41. Loffredo L, Marcoccia A, Pignatelli P, Andreozzi P, Borgia MC, Cangemi R, et al. Oxidative-stress-mediated arterial dysfunction in patients with peripheral arterial disease. Eur Heart J. 2007;28(5):608–12. [PubMed: 17298965]
42. Bradham DM, Igarashi A, Potter RL, Grotendorst GR. Connective tissue growth factor: a cysteine-rich mitogen secreted by human vascular endothelial cells is related to the SRC-induced immediate early gene product CEF-10. J Cell Biol. 1991;114(6):1285–94. [PubMed: 1654338]
43. Tsai CC, Wu SB, Kau HC, Wei YH. Essential role of connective tissue growth factor (CTGF) in transforming growth factor-beta1 (TGF-beta1)-induced myofibroblast transdifferentiation from Graves' orbital fibroblasts. Sci Rep. 2018;8(1):7276. [PubMed: 29739987]
44. Matsuda S, Gomi F, Katayama T, Koyama Y, Tohyama M, Tano Y. Induction of connective tissue growth factor in retinal pigment epithelium cells by oxidative stress. Jpn J Ophthalmol. 2006;50(3):229–34. [PubMed: 16767377]
45. Pi L, Shenoy AK, Liu J, Kim S, Nelson N, Xia H, et al. CCN2/CTGF regulates neovessel formation via targeting structurally conserved cystine knot motifs in multiple angiogenic regulators. FASEB J. 2012;26(8):3365–79. [PubMed: 22611085]
46. Mermis J, Gu H, Xue B, Li F, Tawfik O, Buch S, et al. Hypoxia-inducible factor-1 alpha/platelet derived growth factor axis in HIV-associated pulmonary vascular remodeling. Respir Res. 2011;12:103. [PubMed: 21819559]
47. Worth NF, Rolfe BE, Song J, Campbell GR. Vascular smooth muscle cell phenotypic modulation in culture is associated with reorganisation of contractile and cytoskeletal proteins. Cell Motil Cytoskeleton. 2001;49(3):130–45. [PubMed: 11668582]
48. Branchetti E, Poggio P, Sainger R, Shang E, Grau JB, Jackson BM, et al. Oxidative stress modulates vascular smooth muscle cell phenotype via CTGF in thoracic aortic aneurysm. Cardiovasc Res. 2013;100(2):316–24. [PubMed: 23985903]
49. Ostriker A, Horita HN, Poczobutt J, Weiser-Evans MC, Nemenoff RA. Vascular smooth muscle cell-derived transforming growth factor-beta promotes maturation of activated, neointima lesion-like macrophages. Arteriosclerosis, thrombosis, and vascular biology. 2014;34(4):877–86.
50. Meng XM, Nikolic-Paterson DJ, Lan HY. TGF-beta: the master regulator of fibrosis. Nat Rev Nephrol. 2016;12(6):325–38. [PubMed: 27108839]
51. Li M, Qian M, Kyler K, Xu J. Endothelial-Vascular Smooth Muscle Cells Interactions in Atherosclerosis. Front Cardiovasc Med. 2018;5:151. [PubMed: 30406116]
52. Yu J, Zhang Y, Zhang X, Rudic RD, Bauer PM, Altieri DC, et al. Endothelium derived nitric oxide synthase negatively regulates the PDGF-survivin pathway during flow-dependent vascular remodeling. PloS one. 2012;7(2):e31495. [PubMed: 22355372]
53. Hernandez-Aguilera A, Sepulveda J, Rodriguez-Gallego E, Guirro M, Garcia-Heredia A, Cabre N, et al. Immunohistochemical analysis of paraoxonases and chemokines in arteries of patients with peripheral artery disease. Int J Mol Sci. 2015;16(5):11323–38. [PubMed: 25993297]
54. Chaparala RP, Orsi NM, Lindsey NJ, Girn RS, Homer-Vanniasinkam S. Inflammatory profiling of peripheral arterial disease. Ann Vasc Surg. 2009;23(2):172–8. [PubMed: 18657386]
55. Signorelli SS, Fiore V, Malaponte G. Inflammation and peripheral arterial disease: the value of circulating biomarkers (Review). Int J Mol Med. 2014;33(4):777–83. [PubMed: 24535646]

Author Manuscript Author Manuscript Author Manuscript Author Manuscript

56. Mittal M, Siddiqui MR, Tran K, Reddy SP, Malik AB. Reactive oxygen species in inflammation and tissue injury. Antioxid Redox Signal. 2014;20(7):1126–67. [PubMed: 23991888]

57. Zanoli L, Rastelli S, Inserra G, Castellino P. Arterial structure and function in inflammatory bowel disease. World J Gastroenterol. 2015;21(40):11304–11. [PubMed: 26523102]

58. Smith CW. Endothelial Adhesion Molecules and Their Role in Inflammation. Can J Physiol Pharm. 1993;71(1):76–87.

59. Huang RB, Eniola-Adefeso O. Shear stress modulation of IL-1beta-induced E-selectin expression in human endothelial cells. PLoS One. 2012;7(2):e31874. [PubMed: 22384091]

Author Manuscript Author Manuscript Author Manuscript Author Manuscript

Research in context:

Evidence before this study:

Previous studies in gastrocnemius biopsies from peripheral artery disease (PAD) patients showed that transforming growth factor beta 1 (TGF-β1), the most potent inducer of pathological fibrosis, is increased in the vasculature of PAD patients and correlated with collagen deposition. However, the exact cellular source of TGF-β1 remained unclear.

Added value of this study:

Exposing cells to cycles of normoxia-hypoxia-hyperoxia (NHH) resulted in pathological changes that are consistent with human PAD. This supports the idea that the use of NHH may be a reliable, novel *in vitro* model of PAD useful for studying associated pathophysiological mechanisms. Furthermore, pro-fibrotic factors (PDGF-BB and CTGF) released from endothelial cells were shown to induce a fibrotic phenotype in smooth muscle cells. This suggests a potential interaction between these cell types in the microvasculature that drives increased TGF-β1 expression and collagen deposition. Thus, targeting these pro-fibrotic factors may be an effective strategy to combat fibrosis in response to cycles of ischemia-reperfusion.

Author Manuscript Author Manuscript Author Manuscript Author Manuscript

Highlights

- Cycles of normoxia-hypoxia-hyperoxia increase ROS production by endothelial cells
- Normoxia-hypoxia-hyperoxia cycles increase endothelial cell PDGF-BB and CTGF
- Endothelial cell-derived PDGF-BB and CTGF increase TGF-β in smooth muscle cells

Author Manuscript Author Manuscript Author Manuscript Author Manuscript

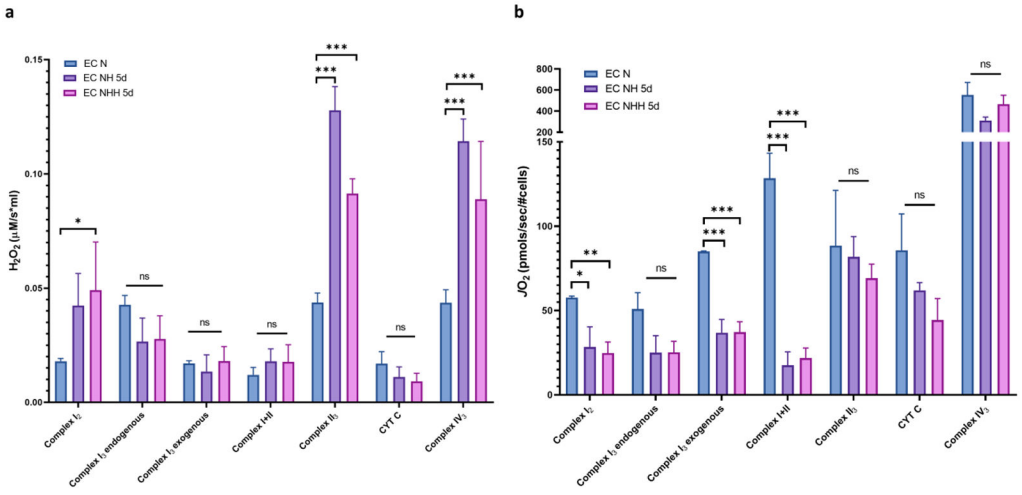

Figure 1: Cycles of NH and NHH reduce oxygen consumption rate and increase H2O2 production in ECs

(a) H_2O_2 production rate, (b) Oxygen consumption rate ($JO2$). Ns represents no significant difference between groups ($p>0.05$), results of ANOVA post-hoc analyses (Bonferroni) displayed as: ns: no significant difference ($p>0.05$), *: $p<0.05$, **: $p<0.01$, and ***: $p<0.001$.

Author Manuscript Author Manuscript Author Manuscript Author Manuscript

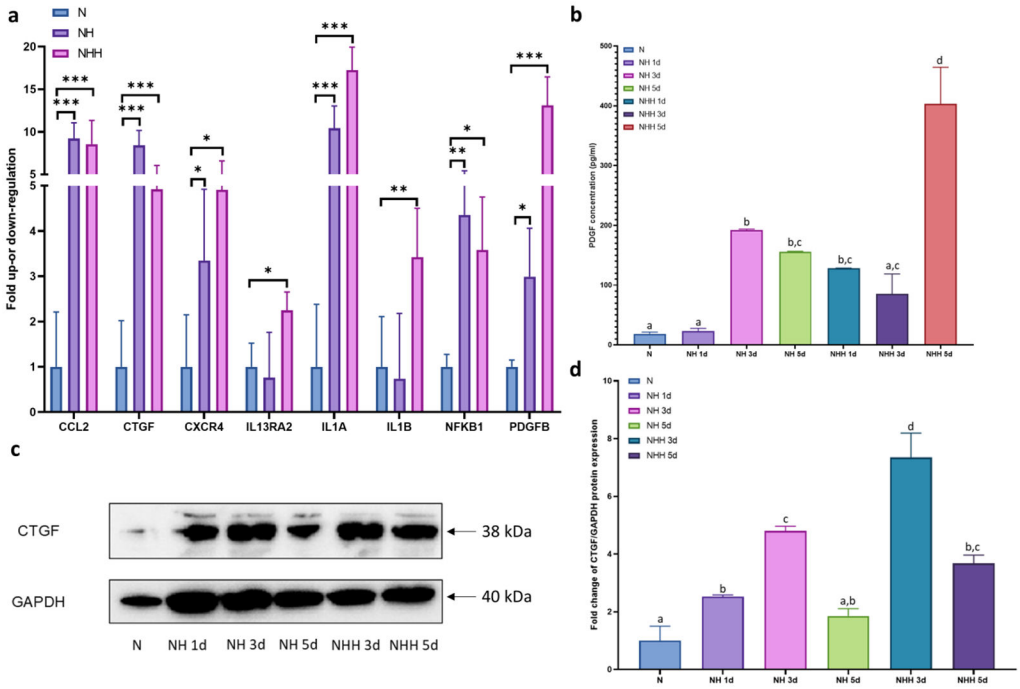

Figure 2: Cycles of NH and NHH increase pro-fibrotic expression in ECs

(a) Relative fold change of mRNA expression detected by real-time PCR, (b) secreted PDGF-BB concentrations determined by ELISA, results of t-test (treatment group vs. control (N)) displayed as: *: $p<0.05$, **: $p<0.01$, and ***: $p<0.001$, (c) Western blot of protein expression of secreted CTGF, GAPDH used as loading control, (d) fold change of CTGF protein expression, results of ANOVA post-hoc analyses (Bonferroni) displayed as: same letters represent means that do not differ ($p>0.05$), different letters represent means that are significantly different ($p<0.05$).

Author Manuscript Author Manuscript Author Manuscript Author Manuscript

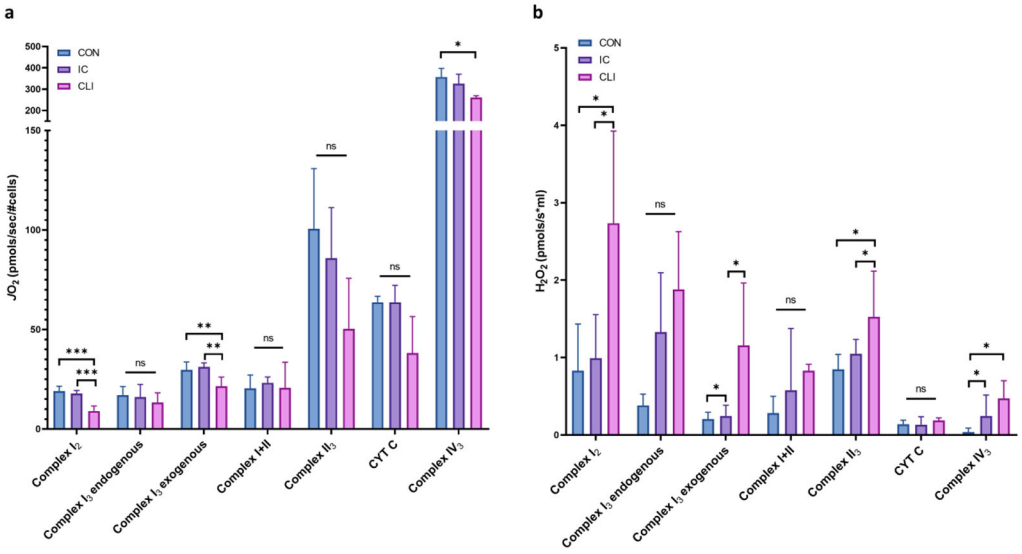

Figure 3: Treatment of SMCs with PAD patient serum increases ROS production

(a) $JO2$, oxygen consumption rate, (b) H_2O_2 production rate, results of ANOVA post-hoc analyses (Bonferroni) displayed as: ns: no significant difference ($p>0.05$), *: $p<0.05$, **: $p<0.01$, and ***: $p<0.001$.

Author Manuscript Author Manuscript Author Manuscript Author Manuscript

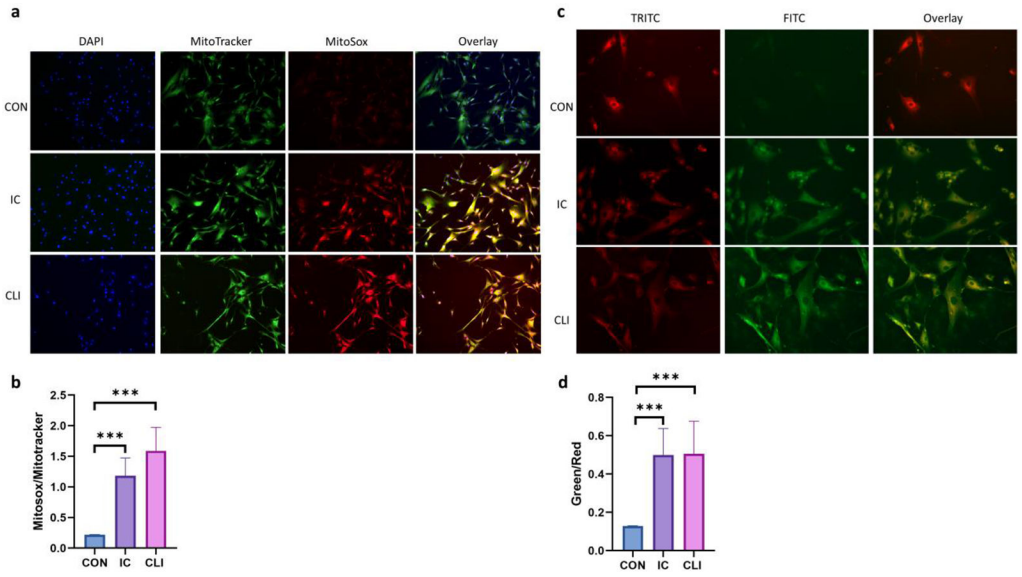

Figure 4: Treatment of SMCs with PAD patient serum increases oxidative damage

(a) Mitochondrial superoxide, immunofluorescence images of SMCs at 40X magnification, Blue: DAPI indicates nuclei, Green: MitoTracker indicates mitochondria for mitochondrial localization, Red: MitoSOX fluorescence indicates mitochondrial superoxide, (b) Average MitoSOX fluorescence relative to MitoTracker, (c) Lipid peroxidation, Immunofluorescence images of SMCs (40X), TRITC (ex/em): 454/600, FITC (ex/em): 490/530, Lipoxite R590/G520 sensor changes from red to green fluorescence upon peroxidation, (d) Average Green/Red fluorescence, results of ANOVA post-hoc analyses (Bonferroni) displayed as: ***: $p<0.001$.

Author Manuscript Author Manuscript Author Manuscript Author Manuscript

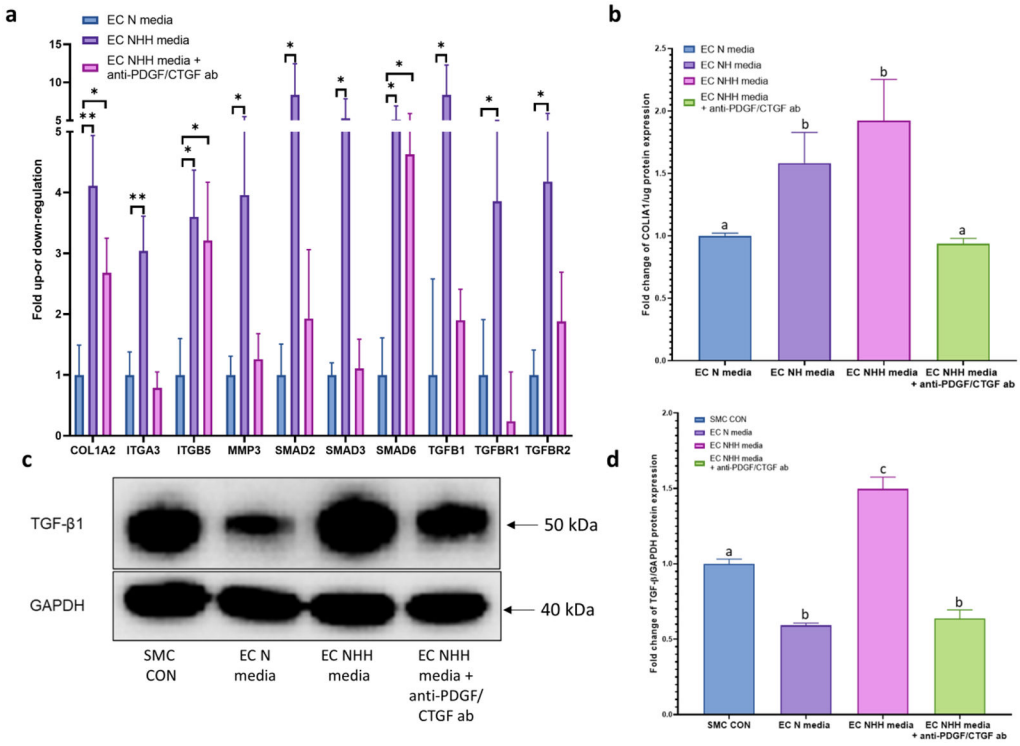

Figure 5: Increased pro-fibrotic expression in SMCs treated with media from ECs undergoing NHH cycles

(a) Relative fold change of mRNA expression detected by real-time PCR, results of t-test (treatment groups vs. control (EC N media)) displayed as: *: $p<0.05$, **: $p<0.01$, (b) fold change of COL1A1 protein expression, (c) Western blot of protein expression of cellular TGF-β1, GAPDH used as loading control, (d) fold change of TGF-β1 expression, results of ANOVA post-hoc analyses (Bonferroni) displayed as: same letters represent means that do not differ ($p>0.05$), different letters represent means that are significantly different ($p<0.05$). SMC CON: control, untreated SMCs, EC N media: SMCs treated with media from ECs cultured under N, EC NHH media: SMCs treated with media from ECs cultured under NHH cycles, EC NHH media + anti-PDGF/CTGF ab: SMCs treated with media from ECs cultured under NHH cycles supplemented with neutralizing antibodies against PDGF-BB and CTGF.

Author Manuscript Author Manuscript Author Manuscript Author Manuscript

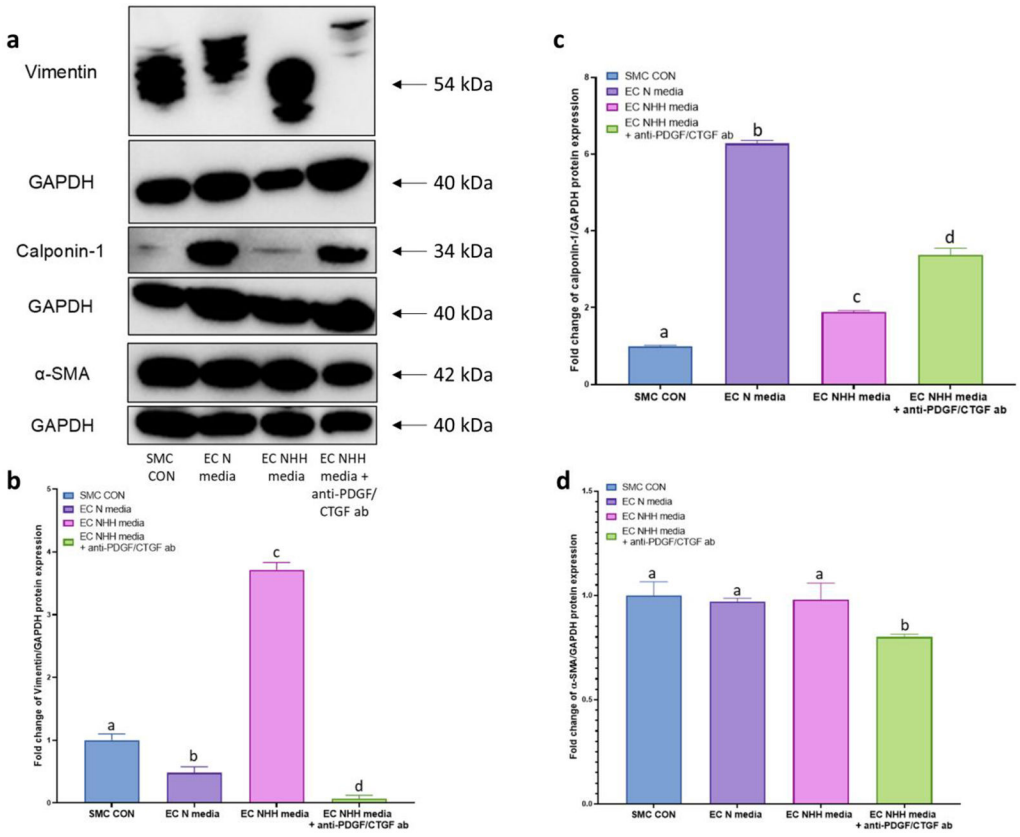

Figure 6: Reduced contractile and increased synthetic markers in SMCs treated with media from ECs undergoing NHH cycles

(a) Western blot of vimentin, calponin-1, and α-SMA, GAPDH used as loading control, (b) fold change of vimentin protein expression, (c) fold change of calponin-1 protein expression, (d) fold change of α-SMA protein expression, results of ANOVA post-hoc analyses (Bonferroni) displayed as: same letters represent means that do not differ ($p>0.05$), different letters represent means that are significantly different ($p<0.05$). SMC CON: control, untreated SMCs, EC N media: SMCs treated with media from ECs cultured under N, EC NHH media: SMCs treated with media from ECs cultured under NHH cycles, EC NHH media + anti-PDGF/CTGF ab: SMCs treated with media from ECs cultured under NHH cycles supplemented with neutralizing antibodies against PDGF-BB and CTGF.

Author Manuscript
Author Manuscript
Author Manuscript
Author Manuscript

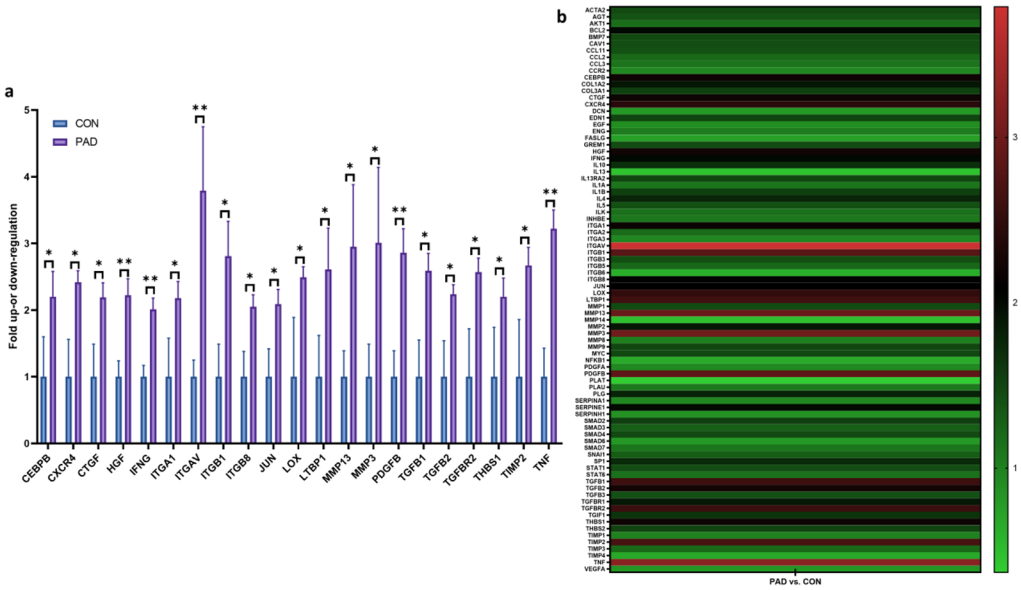

Figure 7: Increased pro-fibrotic gene expression in the gastrocnemius muscle of PAD patients

(a) Relative fold change of mRNA expression of significantly different genes between CON and PAD patients, results of t-test displayed as: *: $p<0.05$, **: $p<0.01$, (b) Heatmap analysis of gastrocnemius tissue expression of fibrosis-related genes, color legend represents calculated relative expression of PAD compared to CON.